

Experimental investigation using acoustic emission technique for quasi-static cracks in steel pipes assessment.

SHEHADEH, M., OSMAN, A., ELBATRAN, A.A., STEEL, J. and REUBEN, R.

2021

© 2021 by the authors. Licensee MDPI, Basel, Switzerland. This article is an open access article distributed under the terms and conditions of the Creative Commons Attribution (CC BY) license (<http://creativecommons.org/licenses/by/4.0/>).

Experimental Investigation Using Acoustic Emission Technique for Quasi-Static Cracks in Steel Pipes Assessment

Mohamed Shehadeh ^{1,2}, Ahmed Osman ¹, Aly Abdelbaky Elbatran ^{1,*}, John Steel ² and Robert Reuben ²

¹ Marine Engineering Department, College of Engineering and Technology, Arab Academy of Science, Technology and Maritime Transport, Abu Kir, Alexandria 1029, Egypt; ezzfahmy@aast.edu (M.S.); ahmed.osman@aast.edu (A.O.)

² Mechanical Engineering, School of Engineering and Physical Sciences, Heriot-Watt University, Edinburgh EH14 4AS, UK; j.a.steel@rgu.ac.uk (J.S.); r.reuben@hw.ac.uk (R.R.)

* Correspondence: a.elbatran@aast.edu; Tel.: +20-111-122-8845

Abstract: Acoustic emission (AE) is a phenomenon where transient waves of stress are generated during deformed material, which is applied to detect and monitor the cracks and cracks propagation. The majority of related literature studied simulated wave sources, which were utilized for a single point of a pipe and have been strictly controlled by temporal characteristics. Therefore, the realistic wave sources which do not have known temporal characteristics are studied in the present work. The realistic source is quasi-static crack propagation under three-point bending. The distortions of AE signals are experimentally evaluated by testing the AE signals of crack propagation using simulated sources. A variety of stress intensities are applied on a steel pipe to determine the effect of stress type and intensity on the characteristics of the source using time and frequency domains. Sensors are mounted on the steel pipe to locate and reconstitute the features of time and frequency domain of the AE sources. It is concluded that the AE energy was sensitive to the crack size which was concerning to the transition of plane-stress to plane-strain. The potential of AE technique for identifying the nature, intensity and location of crack propagation is demonstrated.

Keywords: acoustic emission; bending; quasi-static crack



Citation: Shehadeh, M.; Osman, A.; Elbatran, A.A.; Steel, J.; Reuben, R. Experimental Investigation Using Acoustic Emission Technique for Quasi-Static Cracks in Steel Pipes Assessment. *Machines* **2021**, *9*, 73. <https://doi.org/10.3390/machines9040073>

Academic Editors: Antonio J. Marques Cardoso

Received: 15 January 2021
Accepted: 9 March 2021
Published: 29 March 2021

Publisher's Note: MDPI stays neutral with regard to jurisdictional claims in published maps and institutional affiliations.



Copyright: © 2021 by the authors. Licensee MDPI, Basel, Switzerland. This article is an open access article distributed under the terms and conditions of the Creative Commons Attribution (CC BY) license (<https://creativecommons.org/licenses/by/4.0/>).

1. Introduction

Acoustic emission (AE) is one of the most effective and efficient techniques which can be used for monitoring and detecting fracture and fatigue in metals, wood, ceramics, fibre-glass, composites, plastics and concretes [1]. AE detection uses the energy released from the defected structure during its failure and no external energy source is involved, and hence is considered as a passive technology [2,3]. Accordingly, movements within a material can be detected by AE, whilst other techniques have limited detection of geometrical distortions, and hence AE technique has superior capabilities compared to these methods [2]. Many researchers demonstrate that AE is an effective flaw-monitoring technique [4–8].

The AE signals are prone to dispersion and attenuation due to the wave elasticity features [9,10], given that the AE signal propagation in thin plates is dispersive due to the varying phase velocities at which several frequencies are propagated [11–16]. Consequently, the majority of performed AE monitoring tests showed an interest in specimens with thin plate geometries [11,14]. The correlation between AE events count rates and the rates of crack growth in the steel and welded steel of the compact tension specimens under fatigue were outlined in different studies [17,18]. It was concluded that some parameters (e.g., duration, rise time and rise angle) were very sensitive to the crack propagation rate and were beneficial for the transition characteristics of shear failure under conditions of fatigue [19]. For instance, a study utilized a manipulated metal powder drop test on a metal plate and demonstrated that the number of waveform counts generated correlates to the metal particle diameter [18]. It was demonstrated that the structural damage produced

during fatigue can be monitored using the emitted waves which are sensitive to fractural trends [20]. Research studies applied several types of stress concentration (e.g., circular holes) on tensioned steel plates [21]. They reported that the AE event rates increased between the yield and the ultimate tensile strength (UTS); also, the specimens having stress concentrators started emitting waves earlier than those without. It was suggested that the AE waves were concentrated in three triggering activities: around, and just following, yield; in the advanced stages of work hardening approaching the ultimate tensile strength (UTS); and after the UTS, prior to rupture [22]. Hao et al. [23] utilised AE methods to monitor the plastic deformation during a deep drawing process. Uniaxial tensile tests were performed for initial system calibration. A model was developed for Root Mean Square (RMS) AE (essentially the AE energy) that is directly proportional to the product of strain and strain rate and is similar to an approach used by Carolan et al. [24] to model the AE waves released during metal cutting. Dunegan et al. [25] have suggested that the AE generated is associated with the dislocation motion (plastic deformation) in the plastic zone ahead of a crack tip and are credited with the relationship that the total number, N , of AE counts is proportional to the fourth power of the stress intensity factor. Palmer and Heald [26] found that crack-tip plasticity is a crucial AE wave-generating mechanism and have noted that the total emission count is directly related to plastic zone size which was characterised in terms of the Dugdale strip yielding model. Further experiments on notched stainless steel specimens concluded that the power law dependence of the Dunegan crack extension model varies with the specimen's thickness, thus supporting Palmer and Heald's approach to linking AE with the plastic zone size, and hence, plastic yielding fracture mechanics [27]. Earlier studies [28–31] suggested that the linear elastic fracture mechanics demonstrate the released AE energy during fracture and correlate the AE energy to the strain energy release rate (G_c) in brittle fractures. Several researchers agreed that the plastic deformation at the crack tip is similar in the aforementioned static fracture where the degree of crack tip plasticity is substantial with the increase of the plastic zone size, as in low cycle fatigue or with relatively ductile materials [32–34]. Shehadeh et al. were concerned about monitoring pipeline bending and bucking using the AE technique (e.g., references [35,36]). They used cross correlation with the wavelet transform method for AE source localisation in long pipes [37]. Shehadeh et al. established in subsequent tests that utilized a linear array of the AE sensors to locate and reconstitute the time domain signatures of AE sources in pipes [38]. The correlation between AE signal attenuation with a discontinuous steel pipe was examined by Shehadeh et al. [39]. The distortions of AE continuous and semicontinuous sources (i.e., untemporal) were evaluated in time and frequency domains. Moreover, a study [40] introduced a novel strategy of phased array AE localisation by considering the actual trajectory of the propagating elastic waves in order to localise both the defect axial and radial positions.

The continuous AE sources simulate that the crack propagation of steel pipes is investigated and represented in the current study. A set of tests were conducted to extract significant features of the AE signal associated with untemporal sources in a steel pipe using energy in the time domain method. A variety of intensities were simulated during the crack propagation tests and the effects of type and intensity on time and frequency domain characteristics of the source were evaluated.

2. Materials and Methods

The locative and temporal distribution of the AE sources are less controlled compared to that with simulated sources that were examined in the previous studies [37,39]. Subsequently, the present study aims to evaluate the behaviour of the realistic AE sources. The employed realistic source is quasi-static crack propagation under three bending point. The specific nature of the sources was not known prior, but a series of tests were carried out to perform plastic deformation on a steel pipe. This study developed analytical techniques to gather significant characteristics of the AE signals associated with realistic sources.

This was achieved using energy in the time domain methods by taking the propagation characteristics established in the aforementioned studies into account.

The energy associated with an AE signal over a time, t , can be determined as follows:

$$E = \int_0^t v^2(t) dt \quad (1)$$

where $v(t)$ is the amplitude of the AE waveform in volts, t is time in seconds and the AE energy is given in $V^2 \cdot s$.

A universal testing machine was used to perform three-point bending (destructive testing) on predefined locations of five identical steel pipes 1900 mm in length and 7.35 mm in thickness. A couple of AE sensors were mounted on each pipe, where each sensor was axially located 250 mm either side from the mid-span and circumferentially opposite to a machined notch, as shown in Figures 1 and 2. Five different notch sizes (one notch for a single pipe) of varying depth and constant length to depth ratio (10.3) were used as shown in Figure 3.

Commercial broadband AE sensors (Physical Acoustics Micro-80D type) were used to detect AE. These sensors had a fairly flat frequency response but with two bands of relatively high sensitivity at around 150 kHz and 350 kHz and are based on lead zirconate titanate (PZT). The AE sensor converts detected waves propagating through the material under examination into a time varying voltage signal. This AE sensor is omnidirectional and is sensitive over the frequency range from 175 to 1000 kHz, over an operating temperature range from -65 to $+177$ °C. The sensors are 10 mm in diameter and 12 mm high and were held onto the test object surface using in-house-designed magnetic clamps. In order to obtain good coupling of the AE, the surface was kept smooth and clean and silicone grease was used as couplant to fill any gaps caused by surface roughness and eliminate air gaps which might otherwise impair AE transmission.

The experiments in this research were concentrated on acquiring raw AE signals and data acquisition (DAQ) was based on an in-house built desktop PC with a 12-bit, National Instruments (NI), PCI-6115 board. This board can be used to acquire simultaneously the raw AE signal at 10 M samples/s for up to four channels and uses a full-length PCI-6115 slot. It is a multifunction analogue, digital and timing device without on-board switches or jumpers so that it can be configured and calibrated by software.

The uncertainties for the experimental results in different parameters, AE energy, mechanical energy, fracture energy and intensity factor were around 4%, 5%, 3.5% and 4.5%, respectively.

The notches were loaded in three bending point by a universal testing machine of 50 kN, using 1.66 mm/s crosshead speed. Two simple supports 1300 mm apart and 30 mm high supported the pipes. Rubber coating was applied to the supports and the crosshead's indenter to enhance noise reduction. To measure the displacement of the crosshead, a linear variable displacement transformer (LVDT) was mounted on the test rig. A 4-channel data acquisition device was connected to the outputs of the two AE sensors, the LVDT and the machine load cell for synchronised signal recording.

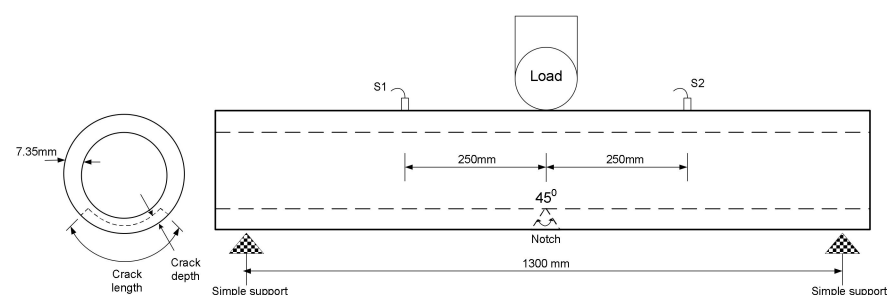


Figure 1. The bending test schematic layout.

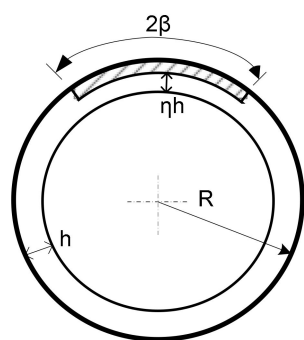


Figure 2. Geometry of circumferential crack.

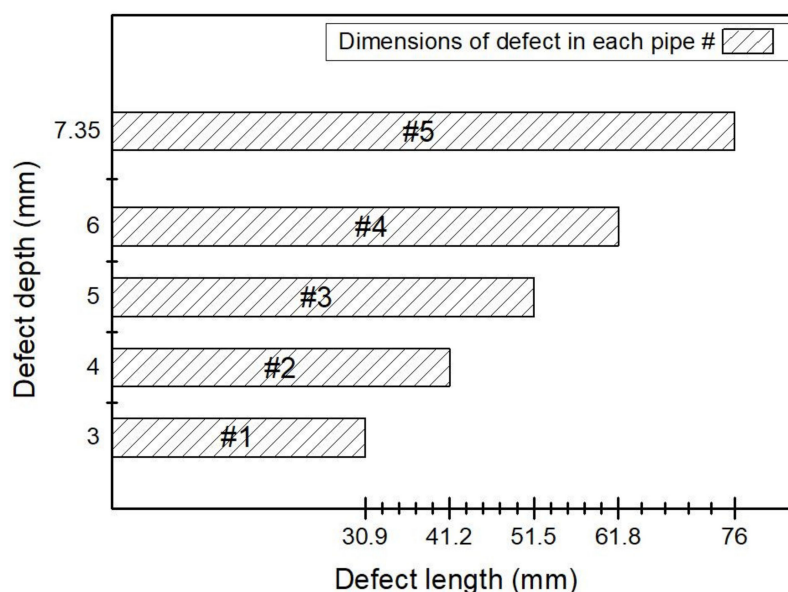


Figure 3. Dimension of the circumferential defect in each pipe.

In the three bending point test, the load is exerted at the mid-span; thus, the bending moment M in the plane of load application can be calculated as the following:

$$M = \frac{Pl}{4} \tag{2}$$

where P is the exerted load and l is the distance between two supports. The notch geometry (in Figure 4) is of an external circumferential defect on a cylindrical pipe under quasi-static loading of bending for which the collapse moment, for $\beta < \frac{\pi}{1+\eta}$ is given by [41]:

$$S_r = \frac{M}{4R^2h\sigma_f} = \cos\left(\frac{(1-\eta)\beta}{2}\right) - \frac{(1-\eta)\sin\beta}{2} \tag{3}$$

where R represents the cylindrical radius (m), M is the bending moment for plastic collapse ($kN.m$), h is the wall thickness, σ_f represents the flow stress which can be taken as the average of the tensile and yield strengths (MPa).

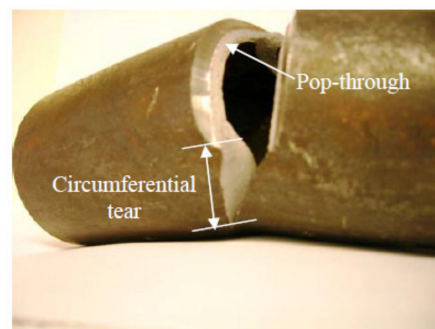


Figure 4. Typical pipe failure from 3-point bending test.

3. Results and Discussion

Processing of frequency and time domains were used to evaluate the raw AE signals and the energy content for all tests. Table 1 shows the calculated moment that caused the collapse and the corresponding geometry of the ligament area in each pipe during the five experiments.

Table 1. Calculated collapse moment and geometry values for the ligament area.

Pipe Number	Collapse Moment (kN·m)	Ligament Length (mm)	ηh (mm)
1	4.75	30.90	4.35
2	4.17	41.20	3.35
3	3.47	51.50	2.35
4	2.95	61.80	1.35
5	1.13	76.00	0.00

The AE signal from the three bending point tests have been recorded at 90 s total time of 1450 batches of 4 ms at a 5 MHz sampling rate. A typical raw AE batch was captured as in Figure 5, while Figure 6 showed a normalised frequency domain plot for the same batch. Unlike the indentation tests, where currently the energy was mostly in a high frequency band at around 350 kHz, some peaks were still visible at a frequency band of 100–150 kHz.

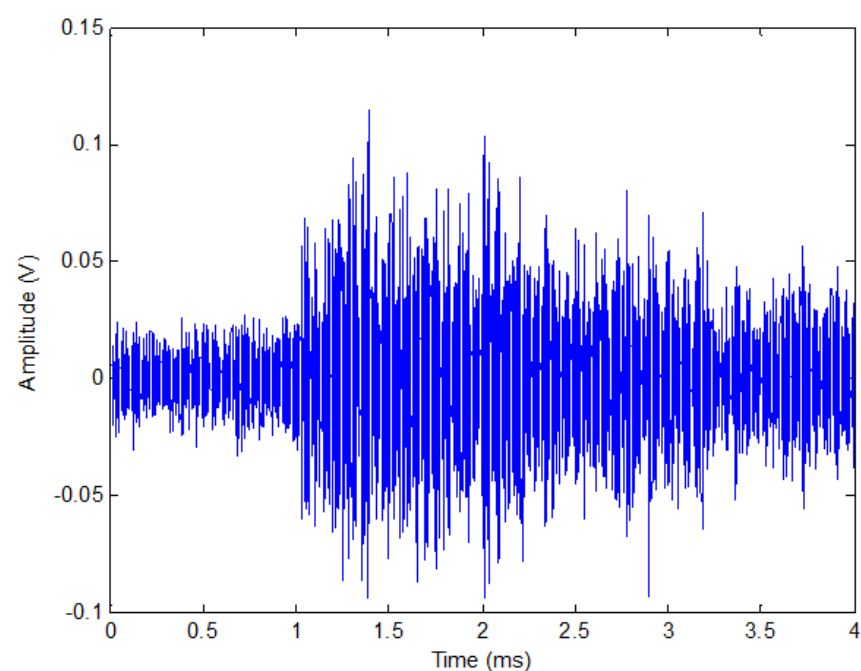


Figure 5. Raw acoustic emission (AE) signal at deflection of 3.22 mm.

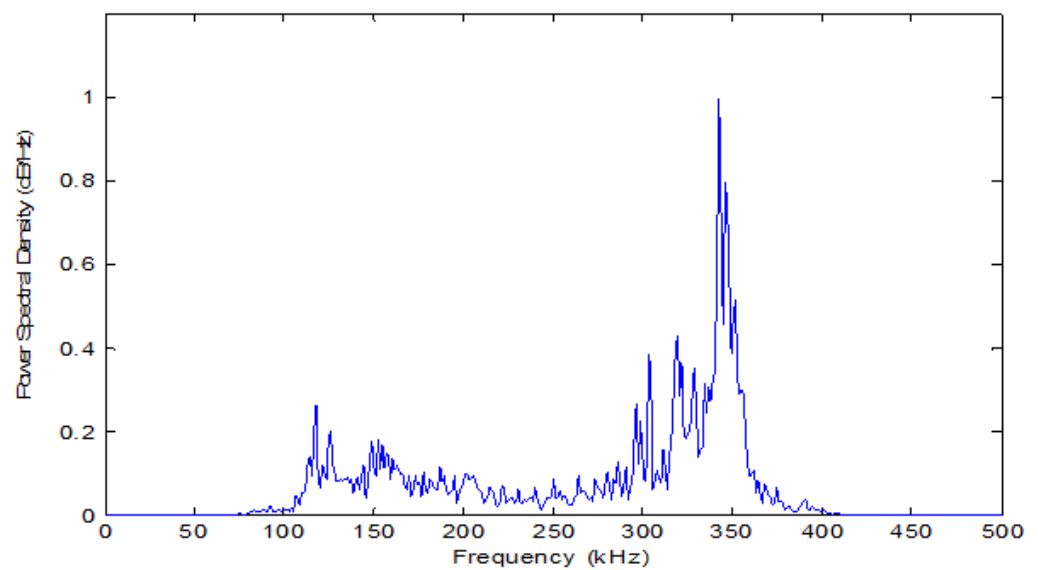
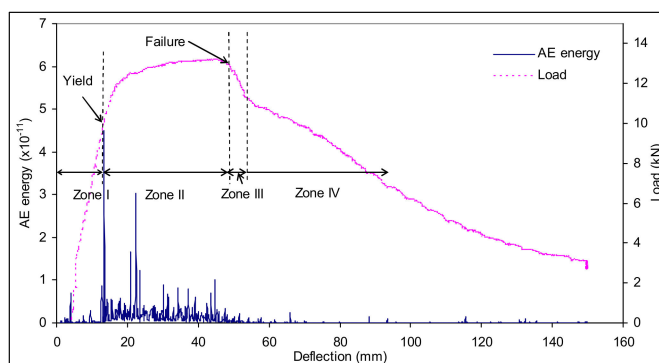


Figure 6. Normalised frequency for pipe 2 at deflection of 3.22 mm.

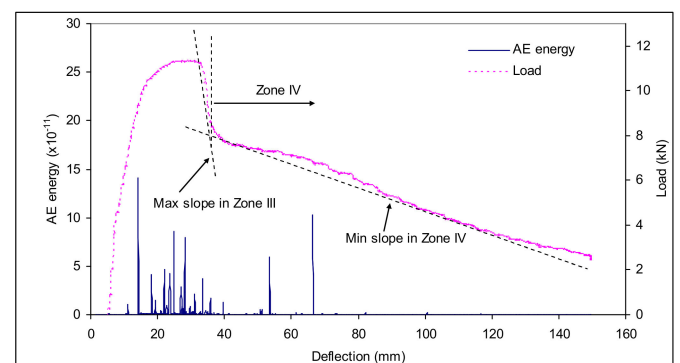
The mechanical notch first cracked through the wall and subsequently propagated around the pipe across its circumference, where the latter was having the features of ductile rupture as opposed to fracture.

As shown in Figure 4, a typical two stage failure of one of the pipes occurs where the mechanical notch first cracks through the wall and subsequently propagates circumferentially around the pipe, the latter having all the features of ductile tearing as opposed to fracture. The maximum moment which was measured from the curve of deflection load versus the calculated collapse moment which was obtained from Equation (2) represents the values of the measured failure moment which are generally higher than that calculated and consistent with the slight underestimate of yield stress as anticipated when using specified values. The smaller the difference for pipes with smaller defects suggests a shift from failure by plastic collapse to failure by fracture at smaller defect sizes.

The load deflection curves for each pipe are demonstrated in Figure 7, with time evolutions of the AE signals (integrated for each batch of 4 ms). Four zones have been generated from the load deflection curves which have a featured shape: pipe elastic deformation (Zone I); Zone II: pipe plastic deformation, expected to be most intense at the notch root; pop-through of a notch (Zone III) which is fast ductile fracture; Zone IV: the popped-through crack extended around the circumference (ductile rupture) and plastic deformation of remaining pipe wall ligation.



(a)



(b)

Figure 7. Cont.

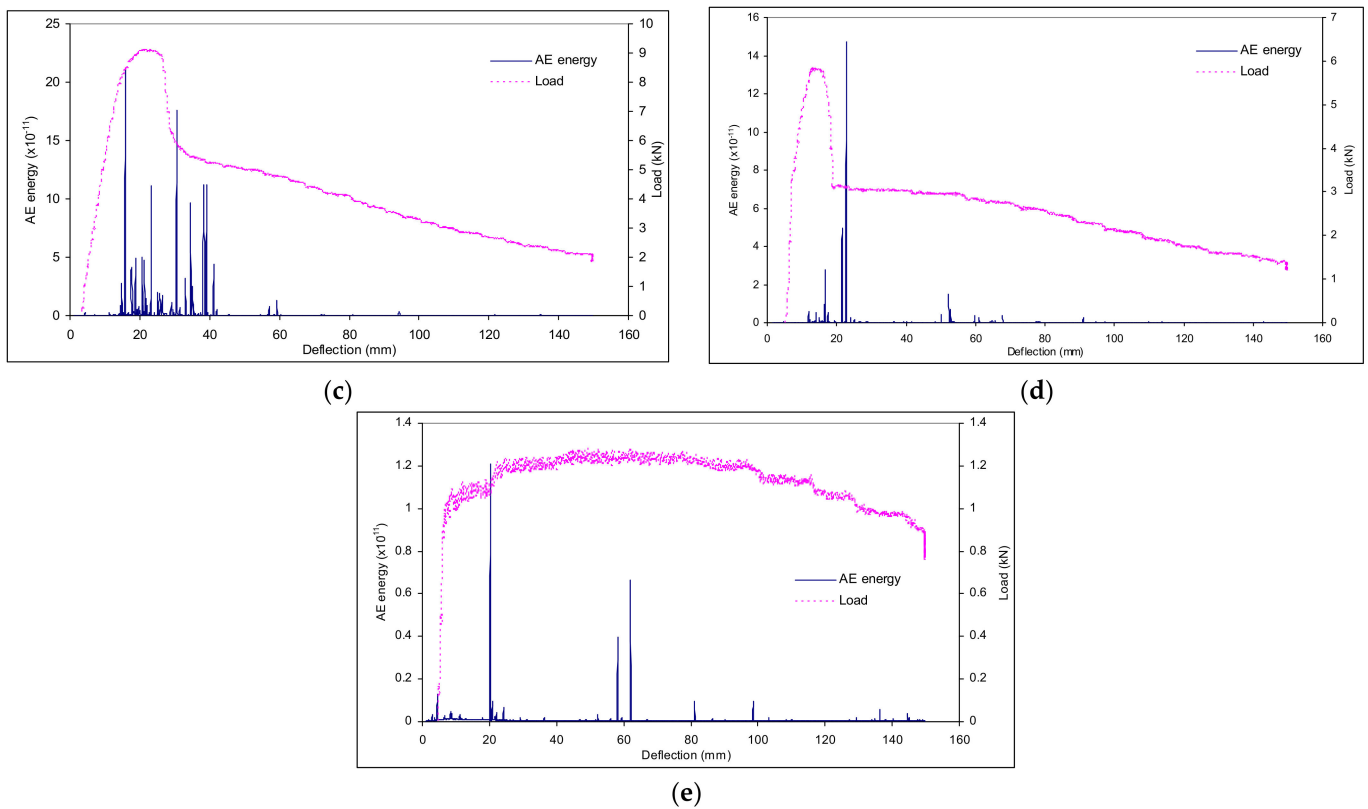


Figure 7. The mechanical load and AE batch energy versus deflection; (a) pipe 1; (b) pipe 2; (c) pipe 3; (d) pipe 4; and (e) pipe 5.

The AE energy is calculated by adding the energy batches for each of the relevant files (defect). The mechanical energy is estimated by calculating the area under the curve of force deflection. The AE and mechanical energies for the entire experiment are shown in Figures 8 and 9 and then split between that up to maximum load (Zones I and II) and that after maximum load (Zones III and IV). It is found that the AE energy for pipe 3 is at a maximum with regards to the total mechanical energy input and that this is associated with the period after maximum load. Zones I and II show an increase in the defect size.

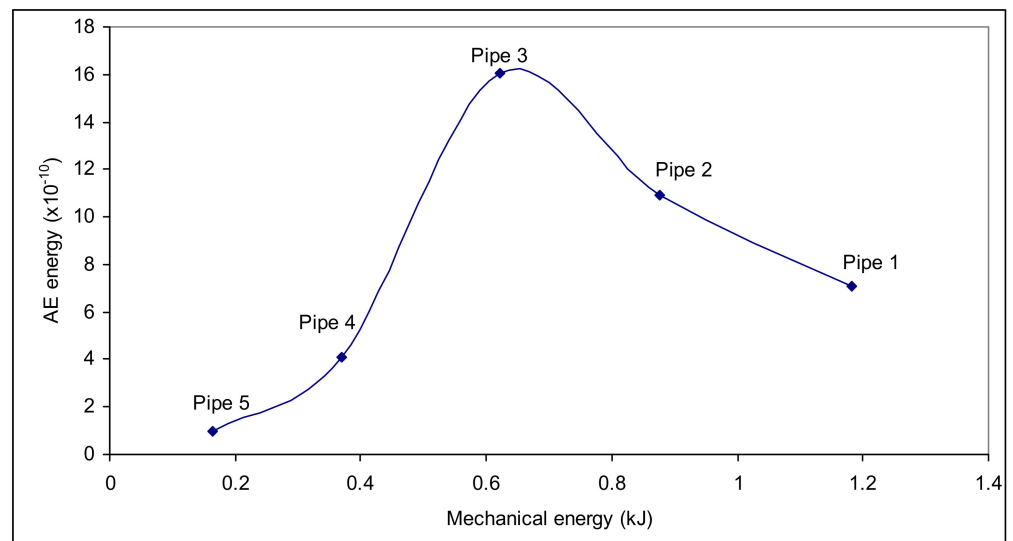


Figure 8. AE energy and mechanical energy.

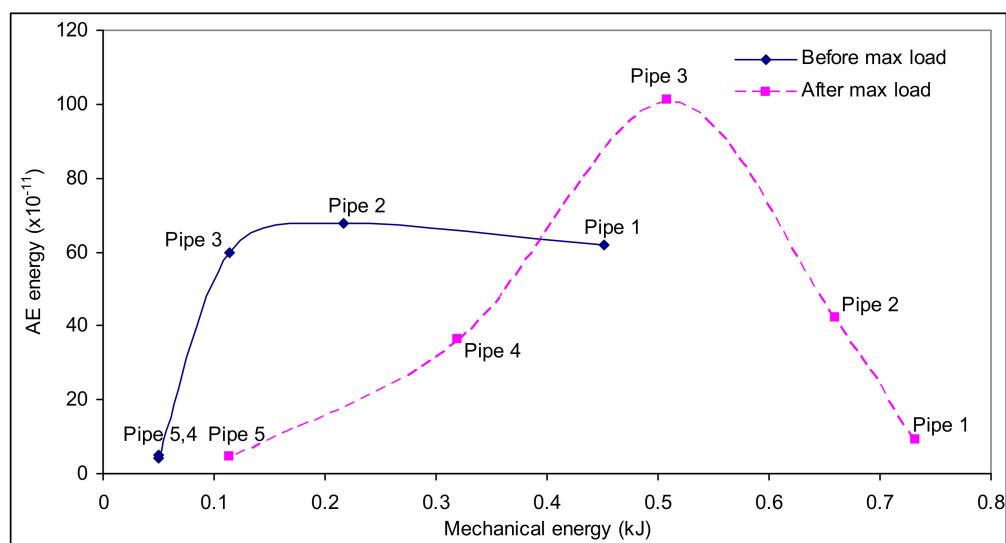


Figure 9. AE energy and mechanical energy before and after maximum load.

There was no considerable change in AE energy in Zones I and II with mechanical energy. However, it dramatically drops off with significantly large defect sizes. The aforementioned observations were caused by the AE signals being sensitive to local deformation, which can be determined by the stress intensity factor, however, were relatively insensitive to the bulk plastic deformation which was the main source of the load resistance. Subsequently, the standard approach in Equation (3) can be used to determine the Mode I stress intensity factor (K_I) for Zones III and IV:

$$K_I = (\gamma\sigma)\sqrt{a\pi} \tag{4}$$

where a represents the depth of notch for Zone III as shown in Figure 10 and circumferential length for Zone IV as shown in Figure 11.

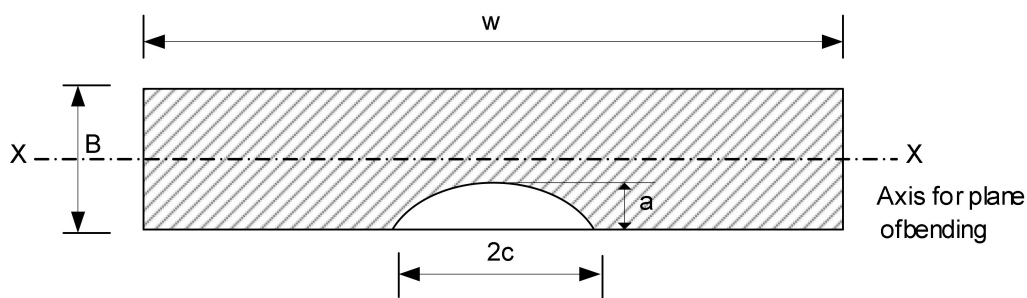


Figure 10. Flaw geometry for Zone III.

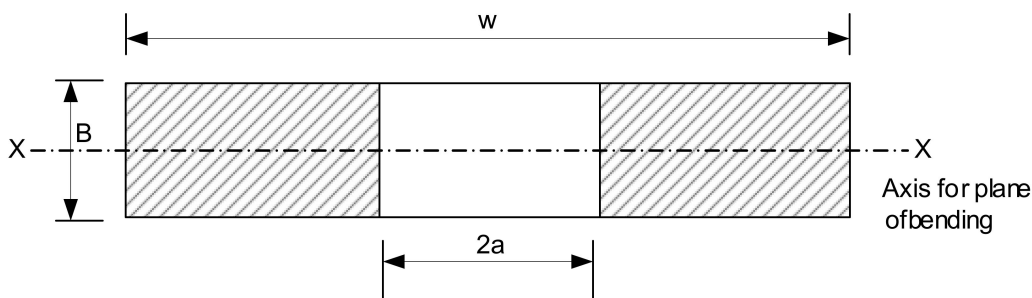


Figure 11. Flaw geometry for Zone IV.

($Y\sigma$) can be determined, taking into account bending stress and membrane, as follows:

$$Y\sigma = Mf_w(\sigma_m M_m + \sigma_b M_b) \quad (5)$$

where M represents correction factor of the bulging, $M = 1$ in this case, and magnification factors are represented by M_m and M_b which can be determined for Zone III from graphs as in reference [42], and for Zone IV ($M_b = M_m = 1$); $\sigma_b = (\sigma_{outer} - \sigma_{inner})/2$ and $\sigma_m = (\sigma_{inner} + \sigma_{outer})/2$ are the bending stress (MPa) and the membrane, respectively; and $f_w = (\sec((a/h)^{0.5}(\pi c/w)^{0.5})$ for Zone III, and $(\sec(a\pi/w))^{0.5}$ for Zone IV, where h is the wall thickness and w is (diameter $\times \pi$), as illustrated in Figures 11 and 12.

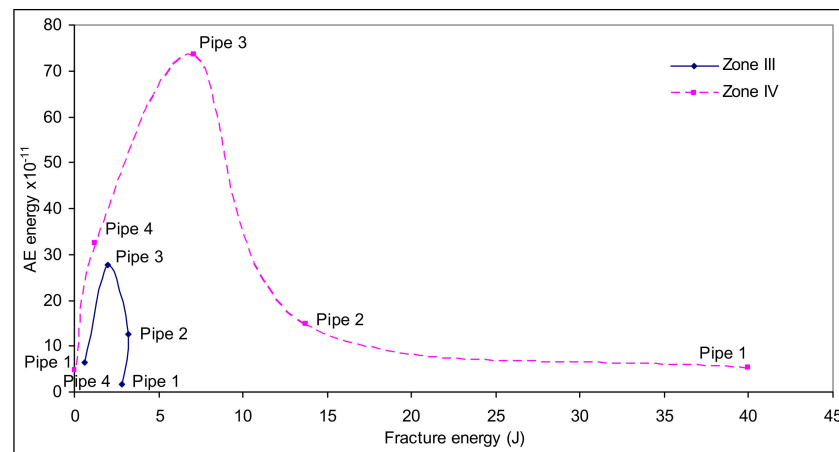


Figure 12. Total AE energy and fracture energy for Zones III and IV.

E_f , the fracture energy, which is associated with the area formation, A , can be determined from G_c , the Griffith toughness, which related to K_I at fracture:

$$E_f = A \times G_c = A \times \frac{K_I^2}{E} \quad (6)$$

where E is the modulus of elasticity. Since the stress at the end of pop-through or ductile tearing are not zero, the Zone III and Zone IV energy of fracture (E_{III} and E_{IV}) can be determined by:

$$E_{III} = A_{lig} \times (G_c^1 - G_c^2) \quad (7)$$

$$E_{IV} = A_{tear} \times (G_c^2 - G_c^3) \quad (8)$$

where A_{lig} and A_{tear} are the areas of pop-through and the ductile tear, respectively; G_c^1 and G_c^2 are the toughness at the start of the fracture process at the end of Zone III and start of Zone IV, respectively, where the toughness at the end of Zone IV is represented as G_c^3 .

Interesting observations can be noticed from the AE energy plotted against two components of fracture energy. Zone III fracture energy was a particularly small proportion of the total mechanical energy. Subsequently, this approach proved that there was a change in the AE energy trends between pipe 1 and pipe 5 that also occurred at pipe 3. The test was conducted for A plane-stress/plane-strain by comparing the product of the yield stress, σ_y , (240 MPa) with the apparent value of K_I and the length of the crack front, L :

$$\frac{K_I^2}{\sigma_y^2 L} \quad (9)$$

where L is the ligament length for pop-through which is given in Table 1 and, for circumferential tearing, L represents the wall thickness of the pipe. Table 2 shows the calculated results of plane-stress/plane-strain results and these should be seen in the context that

the transition from plane-strain to plane-stress took place over a range of $K_I^2/\sigma_y^2 L$ from unity to around 3. Therefore, pipes 3 and 4 can be subject to a process of fracture during pop-through, whereas only pipe 5 was subjected to fracture during the circumferential tearing.

Table 2. Plane-stress/plane-strain results calculated using $\frac{K_I^2}{\sigma_y^2 L}$.

	Pipe 1	Pipe 2	Pipe 3	Pipe 4	Pipe 5
Pop-through	8.22	3.9	1.9	0.6	-
Circumferential tearing	65.5	34.7	19	5.4	0.9

True measures of K_{IC} can be determined for pipe 4 (pop-through) and pipe 5 (circumferential tearing) when $K_I^2/\sigma_y^2 L < 1$ and taking values of K_I at the failure. Consequently, the degree of plasticity of the fracture can be measured by K_I/K_{IC} , which showed interesting findings as shown in Figure 13 when it was plotted against AE energy.

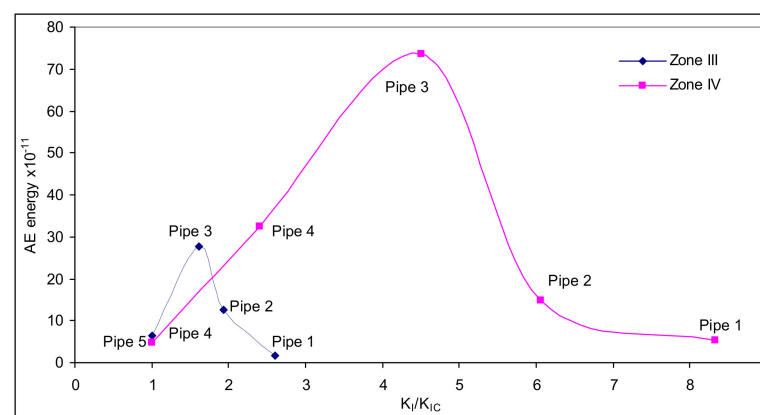


Figure 13. AE energy for Zones III and IV with stress intensity factor.

The plastic deflection in the region prior to maximum load was mostly achieved for pipes 1, 2 and 3 at larger K_I/K_{IC} , in other words, at general yielding in the pipe wall. On the other hand, AE energy appeared less in pipes 4 and 5 with smaller K_I/K_{IC} and the yielding was more confined to the notch area. Two behaviours were created after the maximum load that were based on plasticity of crack propagation degree; thus two groups subsequently appeared, first group: pipes 1, 2 and 3 and second group of pipes 3, 4 and 5. In the first group, the AE energy of pop-through is a relatively small component, a larger one from circumferential tearing and a third from continuous deformation in the pipe wall. Pipe 3 has experienced the least general yielding up to the maximum load; this third component was greater after maximum load than the other two. In pipes 3, 4 and 5, the majority of the AE energy postmaximum load was located in Zone IV and was directly proportional with the tearing energy, which was linearly related to the mechanical energy.

4. Conclusions

The focus of this work was to examine the behaviour of real sources, where the temporal and, to an extent, spatial distribution of the AE source was less controlled than in the case of the simulated sources. The sources chosen were quasi-static crack spreading under three-point bending. The precise nature of the sources was not known a priori but was expected to include crack opening and local general plastic deformation. Consequently, the following findings were derived from the aforementioned study:

- AE due to crack spreading tends to manifest itself mostly in higher frequencies, with contributions from general plastic deformation, and crack spreading by intense plastic deformation and fracture mechanics.

- The cumulative AE energy was mostly produced during periods of intense plastic deformation during the three bending point test, predominantly, the maximum AE energy occurred at the end of Zone I (yield of the pipe section) and the starting of Zone IV (plastic tearing).
- The experiments reported here have spanned the plane-stress/plane-strain transition and, as such, have provided two distinct trends with crack size. The AE energy was sensitive to where the size of crack lay regarding the transition of plane-stress to plane-strain.
- Transitions of the plane-stress to plane-strain have extended and, as such, have supplied two distinct trends with crack size.
- The emitted AE signals due to crack propagation tends to be obvious in higher frequencies, with contributions from general plastic deformation, and the crack propagation by fracture mechanics and extensive plastic deformation.
- The time domain can also clearly be used to recognize between these specific crack sizes.

Author Contributions: Conceptualization, M.S. and R.R.; methodology, M.S., J.S. and R.R.; software, M.S.; validation, M.S.; formal analysis, M.S.; investigation, M.S., J.S. and R.R.; resources, R.R.; data curation, M.S.; writing—original draft preparation, M.S., A.O. and A.A.E.; writing—review and editing, A.O. and A.A.E.; visualization, M.S.; supervision, M.S.; project administration, M.S.; All authors have read and agreed to the published version of the manuscript.

Funding: This research received no external funding.

Institutional Review Board Statement: Not applicable.

Informed Consent Statement: Not applicable.

Data Availability Statement: The data presented in this study are available on request from the corresponding author. The data are not publicly available due to privacy.

Acknowledgments: The authors would also express their gratitude to AE laboratory staff members for their support and guidance in building the test rig.

Conflicts of Interest: The authors declare no conflict of interest.

References

1. Huang, M.; Jiang, L.; Liaw, P.K.; Brooks, C.R.; Seeley, R.; Klarstrom, D.L. Using acoustic emission in fatigue and fracture materials research. *JOM* **1998**, *50*, 1–14.
2. Kaphle, M.R. Analysis of Acoustic Emission Data for Accurate Damage Assessment for Structural Health Monitoring Applications. Ph.D. Thesis, Queensland University of Technology, Brisbane, Australia, 2012.
3. Sheahan, T.; Briens, L. Passive acoustic emission monitoring of pellet coat thickness in a fluidized bed. *Powder Technol.* **2015**, *286*, 172–180. [[CrossRef](#)]
4. Buckley, K.; Venkatesan, G.; West, D.; Kaveh, M. Detection and characterization of cracks for failure monitoring and diagnostics. In Proceedings of the 1996 IEEE International Conference on Acoustics, Speech, and Signal Processing Conference Proceedings, Atlanta, GA, USA, IEEE, 9–19 May 1996; pp. 2738–2741. [[CrossRef](#)]
5. Wood, B.; Harris, R. Structural integrity and remnant life evaluation of pressure equipment from acoustic emission monitoring. *Int. J. Press. Vessel. Pip.* **2000**, *77*, 125–132. [[CrossRef](#)]
6. Von Stebut, J. Multi-mode scratch testing—a European standards, measurements and testing study. *Surf. Coat. Technol.* **2005**, *200*, 346–350. [[CrossRef](#)]
7. Boyd, J.W.; Varley, J. The uses of passive measurement of acoustic emissions from chemical engineering processes. *Chem. Eng. Sci.* **2001**, *56*, 1749–1767. [[CrossRef](#)]
8. Richter, H.; Böhmert, J.; Viehrig, H.-W. The use of acoustic emission to determine characteristic dynamic strength and toughness properties of steel. *Nucl. Eng. Des.* **1999**, *188*, 241–254. [[CrossRef](#)]
9. Shehadeh, M.; Abdou, W.; Steel, J.A.; Reuben, R.L. Aspects of acoustic emission attenuation in steel pipes subject to different internal and external environments. *Proc. Inst. Mech. Eng. Part E J. Process. Mech. Eng.* **2008**, *222*, 41–54. [[CrossRef](#)]
10. Kim, Y.H.; Lee, S.; Kim, H.C. Attenuation and dispersion of elastic waves in multi-phase materials. *J. Phys. D Appl. Phys.* **1991**, *24*, 1722–1728. [[CrossRef](#)]
11. Aggelis, D.G.; Matikas, T.E. Effect of plate wave dispersion on the acoustic emission parameters in metals. *Comput. Struct.* **2012**, *98–99*, 17–22. [[CrossRef](#)]

12. Sedlák, P.; Hirose, Y.; Khan, S.A.; Enoki, M.; Sikula, J. New automatic localization technique of acoustic emission signals in thin metal plates. *Ultrasonics* **2009**, *49*, 254–262. [[CrossRef](#)]
13. Brepta, R.; Vales, F.; Červ, J.; Tikal, B. Rayleigh wave dispersion due to spatial (FEM) discretization of a thin elastic solid having non-curved boundary. *Comput. Struct.* **1996**, *58*, 1233–1244. [[CrossRef](#)]
14. Rose, J. Interface waves. In *Ultrasonic Waves in Solid Media*; Cambridge University Press: Cambridge, CA, USA, 2004; pp. 132–135.
15. Brown, J.A.; Vendra, L.J.; Rabiei, A. Bending Properties of Al-Steel and Steel-Steel Composite Metal Foams. *Met. Mater. Trans. A* **2010**, *41*, 2784–2793. [[CrossRef](#)]
16. Hoang, T.D.; Herbelot, C.; Imad, A. Rupture and damage mechanism analysis of a bolted assembly using coupling techniques between A.E. and D.I.C. *Eng. Struct.* **2010**, *32*, 2793–2803. [[CrossRef](#)]
17. Roberts, T.; Talebzadeh, M. Acoustic emission monitoring of fatigue crack propagation. *J. Constr. Steel Res.* **2003**, *59*, 695–712. [[CrossRef](#)]
18. Boschetto, A.; Quadrini, F. Powder size measurement by acoustic emission. *Measurement* **2011**, *44*, 290–297. [[CrossRef](#)]
19. Aggelis, D.; Kordatos, E.; Matikas, T. Acoustic emission for fatigue damage characterization in metal plates. *Mech. Res. Commun.* **2011**, *38*, 106–110. [[CrossRef](#)]
20. Han, Z.; Luo, H.; Cao, J.; Wang, H. Acoustic emission during fatigue crack propagation in a micro-alloyed steel and welds. *Mater. Sci. Eng. A* **2011**, *528*, 7751–7756. [[CrossRef](#)]
21. Singh, S.K.; Srinivasan, K.; Chakraborty, D. Acoustic emission studies on metallic specimen under tensile loading. *Mater. Des.* **2003**, *24*, 471–481. [[CrossRef](#)]
22. Baudouin, P.; Houbaert, Y. The study of a uniaxial deformation effect on the magnetic properties of a non-oriented electrical steel using acoustic emission characterization. *J. Magn. Magn. Mater.* **2002**, *246*, 247–253. [[CrossRef](#)]
23. Hao, S.; Ramalingam, S.; Klamecki, B. Acoustic emission monitoring of sheet metal forming: Characterization of the transducer, the work material and the process. *J. Mater. Process. Technol.* **2000**, *101*, 124–136. [[CrossRef](#)]
24. Carolan, T.A.; Kidd, S.R.; Hand, D.P.; Wilcox, S.J.; Wilkinson, P.; Barton, J.S.; Jones, J.D.C.; Reuben, R.L. Acoustic emission monitoring of tool wear during the face milling of steels and aluminium alloys using a fibre optic sensor. Part 2: Frequency analysis. *Proc. Inst. Mech. Eng. Part B J. Eng. Manuf.* **1997**, *211*, 311–319. [[CrossRef](#)]
25. Dunegan, H.; Harris, D.; Teleman, A. Detection of fatigue crack growth by acoustic emission techniques. *Ultrasonics* **1971**, *9*, 124. [[CrossRef](#)]
26. Palmer, I.; Heald, P. The application of acoustic emission measurements to fracture mechanics. *Mater. Sci. Eng.* **1973**, *11*, 181–184. [[CrossRef](#)]
27. Mukhopadhyay, C.; Jayakumar, T.; Raj, B.; Ray, K. The influence of notch on the acoustic emission generated during tensile testing of nuclear grade AISI type 304 stainless steel. *Mater. Sci. Eng. A* **2000**, *276*, 83–90. [[CrossRef](#)]
28. Radon, J.; Pollock, A. Acoustic emissions and energy transfer during crack propagation. *Eng. Fract. Mech.* **1972**, *4*, 295–310. [[CrossRef](#)]
29. Muralidhara, S.; Prasad, B.R.; Eskandari, H.; Karihaloo, B. Fracture process zone size and true fracture energy of concrete using acoustic emission. *Constr. Build. Mater.* **2010**, *24*, 479–486. [[CrossRef](#)]
30. Wu, S.; Ge, H.; Wang, X.; Meng, F. Shale failure processes and spatial distribution of fractures obtained by AE monitoring. *J. Nat. Gas Sci. Eng.* **2017**, *41*, 82–92. [[CrossRef](#)]
31. Sagar, R.V.; Prasad, B.R. An experimental study on acoustic emission energy as a quantitative measure of size independent specific fracture energy of concrete beams. *Constr. Build. Mater.* **2011**, *25*, 2349–2357. [[CrossRef](#)]
32. Lindley, T.; Palmer, I.; Richards, C. Acoustic emission monitoring of fatigue crack growth. *Mater. Sci. Eng.* **1978**, *32*, 1–15. [[CrossRef](#)]
33. Bassim, M.; Houssny-Emam, M. Acoustic emission during the low cycle fatigue of AISI 4340 steel. *Mater. Sci. Eng.* **1984**, *68*, 79–83. [[CrossRef](#)]
34. Hartbower, C.E.; Morais, C.F.; Reuter, W.G.; Crimmins, P. Acoustic emission from low-cycle high-stress-intensity fatigue. *Eng. Fract. Mech.* **1973**, *5*, 765–789. [[CrossRef](#)]
35. Shehadeh, M.F.; Abdel Geliel, M.; El-Araby, A. Buckling detection within subsea pipeline laying using Acoustic Emission technique. In Proceedings of the 29th European Conference on Acoustic Emission Testing (EWGAE), Vienna, Austria, 8–10 September 2010.
36. Abdel-Geliel, M.; Shehadeh, M.F.; El-Araby, A. Pipeline bending detection using Acoustic Emission system. In Proceedings of the 17th International congress on sound and vibration (ICSV), Cairo, Egypt, 18–22 July 2010.
37. Shehadeh, M.; Elghamry, M.; Steel, J.A.; Reuben, R.L. AE source location in long steel pipes using cross-correlation and wavelet transforms. In Proceedings of the 17th Congress of Condition Monitoring and Diagnostic Engineering Management, COMADEM, Cambridge, UK, 2–5 July 2004; pp. 250–259.
38. Shehadeh, M.; Steel, J.A.; Reuben, R.L. Acoustic Emission Source Location for Steel Pipe and Pipeline Applications: The Role of Arrival Time Estimation. *Proc. Inst. Mech. Eng. Part E J. Process. Mech. Eng.* **2006**, *220*, 121–133. [[CrossRef](#)]
39. Shehadeh, M.F.; Elbatran, A.H.; Mehanna, A.; Steel, J.A.; Reuben, R.L. Evaluation of Acoustic Emission Source Location in Long Steel Pipes for Continuous and Semi-continuous Sources. *J. Nondestruct. Eval.* **2019**, *38*, 40. [[CrossRef](#)]
40. Zhang, L.; Enpei, C.; Okudan, G.; Ozevin, D. Phased Acoustic Emission Sensor Array for Determining Radial and Axial Position of Defects in Pipe-like Structures. *J. Acoust. Emiss.* **2019**, *36*, 1–2.

-
41. Miller, A. Review of limit loads of structures containing defects. *Int. J. Press. Vessel. Pip.* **1988**, *32*, 197–327. [[CrossRef](#)]
 42. British Standard. *Guidance on Methods for Assessing the Acceptability of Flaws in Metallic Structures*. BS 7910; British Standard Institution: London, UK, 1999; pp. 157–165.